Signaling in Small Subcellular Volumes. I. Stochastic and Diffusion Effects on Individual Pathways

Upinder S. Bhalla
National Centre for Biological Sciences, Tata Institute of Fundamental Research, GKVK Campus, Bangalore, India

ABSTRACT Many cellular signaling events occur in small subcellular volumes and involve low-abundance molecular species. This context introduces two major differences from mass-action analyses of nondiffusive signaling. First, reactions involving small numbers of molecules occur in a probabilistic manner which introduces scatter in chemical activities. Second, the timescale of diffusion of molecules between subcellular compartments and the rest of the cell is comparable to the timescale of many chemical reactions, altering the dynamics and outcomes of signaling reactions. This study examines both these effects on information flow through four protein kinase regulatory pathways. The analysis uses Monte Carlo simulations in a subcellular volume diffusively coupled to a bulk cellular volume. Diffusion constants and the volume of the subcellular compartment are systematically varied to account for a range of cellular conditions. Each pathway is characterized in terms of the probabilistic scatter in active kinase levels as a measure of "noise" on the pathway output. Under the conditions reported here, most signaling outcomes in a volume below one femtoliter are severely degraded. Diffusion and subcellular compartmentalization influence the signaling chemistry to give a diversity of signaling outcomes. These outcomes may include washout of the signal, reinforcement of signals, and conversion of steady responses to transients.

INTRODUCTION

Most current analyses of cellular signaling rely on mass-action kinetics with an implicit assumption that molecular concentrations are continuous. This leads to deterministic solutions of systems of differential equations that describe mass-action kinetics. However, many cellular signaling events involve small numbers of molecules and should be analyzed using stochastic calculations (Gillespie, 1977; Rao et al., 2002). In such situations the outcome of any given experiment can only be stated in probabilistic terms. Further, the chemical output fluctuates even at timescales much greater than the equilibration timescale as calculated according to mass-action kinetics (Rao et al., 2002).

Several calculations of signaling events have been performed using stochastic methods. Stochasticity in signaling can both enhance sensitivity (Paulsson et al., 2000) as well as reduce the sharpness of thresholding responses (Berg et al., 2000). Many studies on gene expression and regulation consider stochasticity, which is clearly important given the small number of participating molecules (Arkin et al., 1998; Kepler and Elston, 2001; Kierzek et al., 2001; Thattai and van Oudenaarden, 2001; Elowitz et al., 2002; Ozbudak et al., 2002). Chemotaxis has been studied in detail using probabilistic models to account for the switching between forward motion and tumbling (Morton-Firth et al., 1999). The influence of stochasticity on circadian rhythms and oscillators has been examined by several groups (e.g., Gonze et al., 2002; Vilar et al., 2002). These studies show that there are a number of ways in which stochasticity affects cellular computation, primarily in introducing noise and in providing for probabilistic cellular decisions, but also as a mechanism employed as part of signaling computation. Clearly, stochasticity should have an impact on many cellular signaling pathways when small cellular volumes and molecular concentrations are taken into account.

Spatial aspects of cellular signaling have also been the subject of investigation by many groups. Many studies have examined pattern formation through interacting chemical reactions (Harrison, 1993). The propagation of chemical waves, especially in calcium signaling, has been simulated and closely related to experiments (Fink et al., 2000; Strier et al., 2003). Recent experimental techniques have begun to open the way for investigation of signaling effects on the scale of cellular microdomains (Rich et al., 2000) and dendritic spines (Sabatini and Svoboda, 2000; Goldberg et al., 2003). The interaction of diffusion with membrane-localized protein kinase function has been analyzed using computational methods to suggest that diffusion and spatial separation can play a major part in controlling phosphorylation state (Kholodenko et al., 2000; Kholodenko, 2003). Diffusion in these small volumes is particularly interesting as they are also the scale in which stochastic effects become important.

Only a few studies have attempted to combine both the stochastic and diffusive effects. The bacterial chemotaxis system has been the subject of much of this work, examining both the diffusive properties of the signaling molecules and the implications of the spatial organization of receptor arrays (Levin et al., 2002; Shimizu et al., 2003). Resat et al. (2003) have recently considered epidermal growth factor receptor

Submitted January 21, 2004, and accepted for publication April 9, 2004.

Address reprint requests to Upinder S. Bhalla, National Centre for Biological Sciences, TIFR, GKVK Campus, Bangalore 560065, India. Tel.: 91-80-2363-6420 ext. 3230; Fax: 91-80-2363-6662; E-mail: bhalla@ncbs.res.in.

0006-3495/04/08/733/12 $2.00

doi: 10.1529/biophysj.104.040469

(EGFR) activation in a multicompartmental model. Calcium diffusion analyses involving stochasticity have also been performed (e.g., Falcke, 2003). Several studies on synaptic transmission have utilized Brownian motion diffusion along with stochastic chemical interactions (Stiles and Bartol, 2000; Franks et al., 2002).

Here we study the combined effects of stochasticity and diffusion in subcellular regions such as microdomains and dendritic spines. In this paper four major signaling pathways are examined as examples of linear pathway signaling in small diffusively coupled volumes. In the accompanying article, the behavior of the synaptic signaling network, involving these and additional pathways, is examined under similar conditions. The spatial geometry considered is very simple, consisting only of a protuberance attached to a cell of typical volume. The protuberance is assumed to be spatially homogenous. The signaling pathway is modeled identically in both the compartment and the cell. Three parameters are varied in this study: volume of the signaling compartment, the diffusion constant, and the stimulus strength. The pathways are modeled at a moderate level of chemical detail, including some aspects of partitioning of molecules between cytosol and membrane. Rate constants and concentrations for the reactions are from biochemical experiments reported in the literature, and are mostly from neuronal preparations. The study shows that both stochastic and diffusive effects strongly limit the kinds of signals that could usefully be transformed in small subcellular volumes. On these scales the diffusive time courses are comparable to reaction rates. This frequently leads to contrasting signaling outcomes that arise for the same pathway depending on geometry and diffusion constants. Compartmentalization, such as membrane anchoring, leads to interesting interactions with diffusive effects.

METHODS

Simulation models were derived closely from those used previously to study temporal tuning by signaling networks, which in turn are based on biochemical parameters and molecular concentrations mined from the biochemical literature, mostly using neuronal tissue sources (Bhalla, 2002a). Detailed reaction schemes are given for each of the pathways analyzed. Each of the models has been uploaded to the DOQCS database (Sivakumaran et al., 2003) as accessions 47, 48, 49, and 58. Demonstration scripts for replicating the tests are accessible from within the accessions.

Simulations were performed on a 32-CPU Athlon cluster (Atipa Systems, Lawrence, KS) running GENESIS/kinetikit (Bhalla, 1998, 2002b) on the Linux operating system. Deterministic computations were performed using the Exponential Euler method (MacGregor, 1987; Bower and Beeman, 1998). Stochastic calculations were performed using an adaptive stochastic method (Vasudeva and Bhalla, 2004). Briefly, this method chooses whether to employ a stochastic or a deterministic calculation of molecule numbers, for each reaction in the model at each time step. If the propensity for a given reaction is large and the number of molecules on either side of the reaction is large, then the reaction is computed using deterministic integration. Otherwise a stochastic computation is used. The method is less efficient than the Gillespie (1977) or Gibson-Bruck (2000) methods for small molecule counts, but its computation times are almost independent of molecule numbers. Thus it is effective in our simulations where a small cellular compartment is coupled to a large cell volume. Source code for the simulator and the Kinetikit interface incorporating all these methods is available at http://www.ncbs.res.in/~bhalla/kkit/download.html. Demonstration simulations, including model parameter files, for generating several of the figures of this article are available at http://www.ncbs.res.in/~bhalla/stochpath/index.html.

The adaptive method is an approximate method, and in these simulations the time steps were chosen to control the numerical error to better than 5%. However, small (<10%) differences in the distribution of molecular counts about the mean may arise from the method. The error analysis is detailed in Vasudeva and Bhalla (2004). In cases where two identical molecules bind to a target (which occurs in three instances in the CaMKII model) the current implementation of the method computes forward reaction propensities as $n^2 \times$ pf rather than $n \times (n-1) \times$ pf. This would introduce an error of 20% for these reactions for the case of basal Calcium in a volume of 0.1 fl (~5 ions of Ca^{2+}); at higher volumes and concentrations the error is smaller.

Compartmentalization of signaling molecules was considered at two levels. First, the entire signaling circuit was duplicated in two diffusively coupled compartments. The simplest possible diffusion system was assumed, where each compartment was internally homogenous and the only diffusive gradient was between the two compartments. The subcellular compartment of interest had a volume which was varied in the range 0.1–1000 fl. This was diffusively coupled to a bulk compartment of 1000 fl to represent the rest of the cell (Fig. 1 *A*). Second, based on experimental information, several molecules were treated as being membrane bound or cytoskeletally anchored. These molecules did not undergo diffusion and were chemically coupled only to reactions within the local compartment.

The flux form of the diffusion equation was represented in terms of first-order reactions between the compartments, and these reactions were also numerically integrated using the same Exponential Euler or adaptive stochastic method as the chemical calculations. N is the number of molecules (#) per unit volume and D is the diffusion constant.

$$\text{Flux} = -D \times dN/dx, \text{ and} \tag{1}$$

$$(d\#/dt)/XA = -D \times d(\#/vol)/dx = -(D/vol) \times d\#/dx, \tag{2}$$

where XA is the cross-sectional area and x is the direction of diffusion. The rate of transfer of molecule A from compartment 1 to 2, ignoring back-flux, is:

$$(dA1)/dt = -(XA \times D/vol1) \times A1/\delta x, \tag{3}$$

where $vol1$ is the volume of compartment 1 and $vol2$ of compartment 2. Here we approximate the local concentration gradient as the local number of molecules divided by the separation between the compartments, δx, and get

$$(dA1)/dt \sim -kf \times A1 + kb \times A2, \tag{4}$$

where

$$kf = (XA \times D/vol1)/\delta x, \tag{5}$$

and

$$kb = (XA \times D/vol2)/\delta x, \tag{6}$$

and $A1$ and $A2$ are the respective numbers of molecule A in compartment 1 and 2. This is the same form as the equations solved by the system for

deterministic and stochastic chemical reactions. Therefore the diffusion was implemented simply as a reaction step with the rate constants assigned as in Eqs. 5 and 6. Using a simple cubic geometry as in Fig. 1 *A*,

$$\delta x = (vol1)^{1/3} \text{ and} \tag{7}$$

$$XA = (vol1)^{2/3}. \tag{8}$$

Values for the effective rates used in the simulations are shown in Fig. 1 *B*.

Molecule counts were scaled linearly from the reference model for a cell of 1000 femtoliters (10^{-15}). Scaling was done by keeping initial concentrations fixed as per the cell model, and converting to molecule counts at the target volume. The diffusion calculations made the assumption that enzyme-substrate complexes were present very transiently, and did not account for their diffusion.

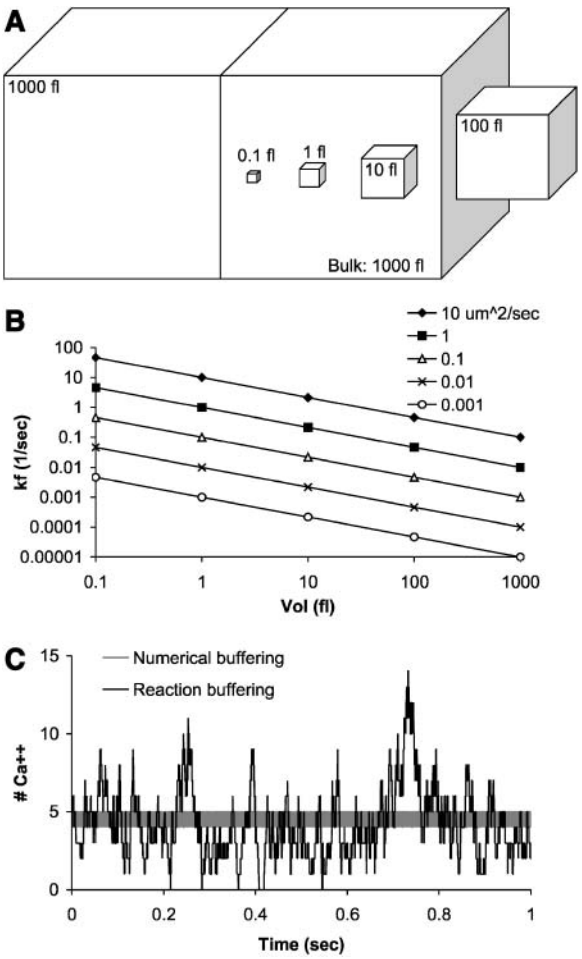

FIGURE 1 Model geometry. (*A*) Configuration of subcellular compartment in diffusive contact with bulk cytosol. Dimensions are approximately to scale, but location of compartments with respect to bulk is arbitrary as each compartment was treated as being in 1-dimensional diffusive contact with the bulk. (*B*) Rate constants k_f for diffusion from compartment to bulk, as per Eq. 5. Rates are comparable to chemical reaction rates. (*C*) Comparison of Ca^{2+} ion distributions for numerical buffering (randomly choosing the integer above or below the target concentration) and reaction buffering as in Fig. 3 *A*. The numerically buffered run (*shaded*) appears as a solid bar because the concentration is recomputed each time step of 0.1 ms, so it fluctuates between 4 and 5 on a finer timescale than can be resolved in the graph. Simulation uses compartment volume of 0.1 fl with a resting $[Ca^{2+}] = 0.08\ \mu M = 4.8$ molecules; and $D = 0.1\ \mu m^2/s$.

Buffering in the deterministic simulations was done by numerically fixing the concentration of the buffered molecule to the desired level. In the case of stochastic simulations, this approach could lead to a fractional number of molecules. This situation was addressed by using a random number generator on each time step to set the number of buffered molecules to the nearest integer above or below the target value, with a probability such that over time the concentration of the molecule averaged to the target value.

Calcium stimuli were treated specially as the molecule is typically subject to a high degree of chelation in the cell. Further, calcium can experience very large concentration gradients with respect to the bulk compartment, leading to diffusional fluxes which also have a noise term. Thus simple numerical buffering as described above would not accurately capture the distribution of calcium ion numbers. To achieve a more accurate distribution of Ca^{2+} levels, the Ca^{2+} input to the subcellular compartment was treated as a simple first order reaction at high rate ($k_f = k_b = 100$/s) from an input source which was numerically buffered as described above (Figs. 3 *A* and 4 *A*). Although this approach ignores the complexity of calcium buffering dynamics, it does produce a more realistic distribution of Ca^{2+} counts in the subcellular compartment as compared to numerical buffering (Fig. 1 *C*).

A parameter named ''settle time'' was computed for each pathway, as an estimate of the time a downstream pathway would have to sample the fluctuating concentration to obtain an accurate readout of the pathway. Taking the stochastic concentration at time t as $S(t)$, and deterministic concentration as $D(t)$, the settling time was reached when the absolute average deviation from the deterministic run was below a certain threshold:

$$\text{Fabs}(\Sigma(S(t) - D(t)))/(D(t) \times (t - t0)) < \text{threshold}. \tag{9}$$

Here samples were taken every second. As this measurement is quite noisy, it was also stipulated that the inequality should hold for 100 consecutive samples. Further, the entire computation was repeated for a range of stimulus values and the settling time averaged to improve the estimate of settling time. The threshold was set to 0.05. When the settling time exceeded the total time of the simulation (typically 4000 s), the algorithm terminated and returned this total time.

RESULTS

Four major kinase pathways: protein kinase A (PKA); protein kinase C (PKC); calcium-calmodulin dependent type II kinase (CaMKII); and the mitogen activated protein kinase (MAPK) were considered. In each case simulations were run for diffusion constants ranging from 0.001 to 10 $\mu m^2/s$ and subcellular compartments with volumes from 0.1 to 1000 fl. Subsets of molecules for each model were treated as nondiffusing based on experimental information about their association with the membrane. The same diffusion constants were used for all remaining molecules in a given run, as specific diffusion data is rarely available for individual molecular species in specific cellular contexts.

Simulations were also run without diffusion, and also using deterministic calculations. Dose-response curves were constructed in response to upstream activators in each case.

PKA

PKA is part of the classical G-protein coupled receptor (GPCR) and cyclic adenosine monophosphate (cAMP) signaling pathway. It exhibits high gain due to multiple enzymatic amplification stages. The PKA activation pathway model included GPCR activation, G-protein responses and adenylyl cyclase (AC) activation, formation of cAMP, and activation of PKA (Fig. 2 *A*). The GPCR and AC activation stages were treated as membrane-bound reactions and did not diffusively exchange with the bulk compartment. The cAMP, PDE, and PKA molecules did experience diffusion. Typical time courses of activation of PKA at a range of diffusion constants are shown using deterministic calculations in Fig. 2 *B*. There is a wide range of steady-state PKA activities, due to diffusive washout of the cAMP and the activated kinase.

When reactions were computed at small volumes (0.1 fl), and stochasticity was considered, the high gain of the PKA pathway led to transient large responses reminiscent of single-channel openings (Fig. 2 *C*). Each such response was much larger than the deterministic value. At larger volumes ($\geq$1 fl) the stochasticity led to responses more closely distributed around the deterministic value (supplementary material).

A series of ligand concentrations was used to generate dose-response curves for PKA, varying the diffusion constant. Higher diffusion rates lower the pathway response (Fig. 2 *D*). The error bars represent standard deviations. A similar series of dose-responses was performed over a range of volumes. As expected, these curves closely tracked the deterministic curve and the standard deviation of the data points increased with smaller volumes (supplementary data).

To quantify the effect of washout, the steady-state value of PKA activity was computed for a range of volumes and diffusion constants (Fig. 2 *E*). In all cases the stimulus was held fixed at 0.1 μM ligand concentration. Washout of the PKA response was severe for a wide range of compartment volumes and diffusion constants. Experimental estimates of cAMP levels suggest that the effective diffusion constants in cAMP signaling microdomains may be very small (Rich et al., 2000).

A critical parameter for information transfer in these small cellular volumes was to estimate the duration for which a downstream pathway should sample the signal to make a good estimate of the activity (Fig. 2 *F*). This was estimated by considering the time it took for the cumulative average of PKA activity to settle to within 5% of the deterministic value, as described in the methods section. The settling time estimate was averaged for four ligand concentrations in the range of 10 nM–100 nM, that is, above the K_{half} for activation of PKA. The settle time for PKA is determined mostly by the compartment volume, and as expected declines sharply at larger volumes.

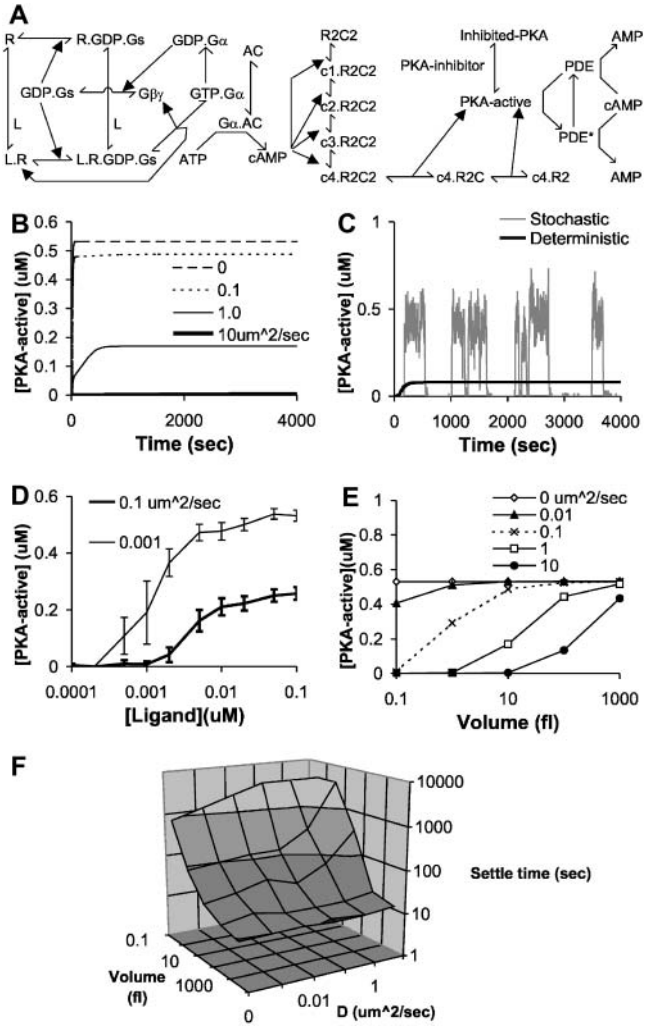

FIGURE 2 PKA responses. Activity of PKA is the concentration of the free catalytic subunit of the enzyme, labeled ''PKA-active'' in the reaction scheme. (*A*) Reaction scheme. The activation step from the ternary complex of ligand, receptor and G-protein to activated GTP.Gα is represented as a lumped step with an implicit exchange of GTP for GDP. Abbreviations: R, receptor; L, ligand; GDP, guanosine diphosphate; GTP, guanosine triphosphate; Gs, G-protein heterotrimer; G$\beta\gamma$, G-protein $\beta\gamma$ complex; Gα, G-protein type s, α subunit; AC, adenylyl cyclase; ATP, adenosine triphosphate; cAMP, cyclic adenosine monophosphate; R2, dimer of protein kinase A regulatory subunit; C2, dimer of protein kinase A catalytic subunit, c1–c4; cAMP with a stoichiometry of 1–4; PDE, phosphodiesterase; and AMP, adenosine monophosphate. (*B*) Time course of simulation responses to a steady input of 0.1 μM ligand, at volume = 10 fl, and a range of diffusion constants. The 10 μm^2/s case undergoes almost complete washout. (*C*) Comparison of stochastic and deterministic runs for identical conditions. Stimulus = 1 nM, volume = 0.1 fl, D = 0.01 μm^2/s. (*D*) Dose-response curves for PKA with different diffusion constants. volume = 1 fl. Error bars are standard deviations. (*E*) Washout as a function of volume and diffusion constant. Stimulus = 0.1 μM ligand. Maximal activity is obtained only when volume is large or diffusion constant small. (*F*) Settling time (defined in methods) as a function of volume and diffusion constant.

PKC

PKC is a ubiquitous kinase that is primarily activated by calcium, but also by arachidonic acid (AA) and

diacylglycerol (DAG). The kinase translocates to the membrane upon activation. The PKC model includes activation by Ca^{2+}, AA, and DAG (Fig. 3 *A*). In this study activation by Ca and AA were considered, and DAG was buffered at its baseline level of 11 μM. As described in the methods, the Ca input was treated as arriving from an external buffered source exchanging with the compartmental Ca. In the PKC model the active forms of PKC (PKC-a1 to PKC-a6) were assumed to be membrane anchored and hence non-diffusive; and the remaining molecules were diffusive. Note that this is the reverse of the situation with PKA, where the input stages were nondiffusive but the output molecules could diffuse.

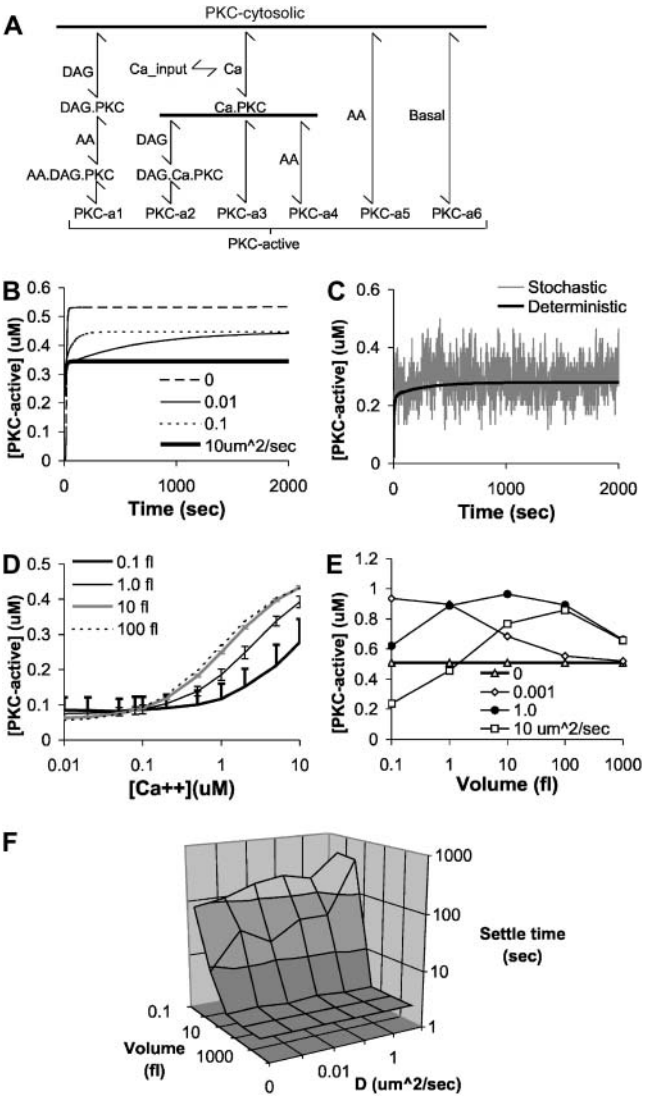

FIGURE 3 PKC responses. (*A*) Reaction scheme. Activity of PKC is the sum of the six differently activated states, PKC-a1 through a6, each of which are treated as membrane-associated. Abbreviations: DAG, diacylglycerol; and AA, arachidonic acid. DAG is held fixed at 11 μM throughout these simulations. (*B*) Time course of simulation responses to an input of 10 μM Ca^{2+} and 5 μM AA, at volume = 10 fl, and a range of diffusion constants. (*C*) Comparison of stochastic and deterministic runs. Stimulus = 1 μM Ca^{2+}, 5 μM AA, volume = 0.1 fl, D = 0.001 $\mu m^2/s$. (*D*) Dose-response curves for PKC with different diffusion constants. Ca is held fixed at 1 μM, volume = 1 fl. Error bars are standard deviations. (*E*) Washout as a function of volume and diffusion constant. A strong stimulus of 10 μM Ca^{2+} and 50 μM AA is applied. Note recruitment as well as washout effects and their dependence on volume and diffusion constant. (*F*) Settling time (defined in methods) as a function of volume and diffusion constant.

The deterministic runs for PKC, like PKA, were monotonically increasing with time (Fig. 3 *B*). The dependence on diffusion constant is complex, affecting both the settling time and the steady-state value of PKC activity. This is due to a competition between washout effects and recruitment to the membrane, which is considered in more detail below (Fig. 3 *E*). As expected, the stochastic runs gave distributions which bracketed the deterministic responses of PKC (Fig. 3 *C*). The degree of scatter appeared to be a function mainly of volume and final level of PKC activity, and did not depend on whether the stimulus was primarily Ca^{2+}, or whether Ca^{2+} and AA were acting synergistically (supplementary data). The activation of PKC as a function of calcium stimulus is shifted to the right at smaller compartmental volumes as expected due to washout of the intermediates in the pathway (Fig. 3 *D*). The standard deviation is not strongly dependent on activity levels. There is the expected trend of smaller standard deviation in signaling outputs with increasing volume (Fig. 3 *D*, supplementary material). The contribution of diffusive stochasticity to the total standard deviation for PKC is quite large, especially at larger volumes.

The PKC model exhibited a transition from diffusive washout of PKC signaling to diffusive recruitment to the membrane (Fig. 3 *E*). At small volumes and rapid diffusive rates, the washout predominates as the reaction intermediates are removed from the compartment more rapidly than they can become membrane-anchored. At intermediate rates of exchange, the recruitment to the membrane predominates, and under these conditions the replacement of PKC-cytosolic from the bulk pool actually increases the total amount of membrane recruitment. Finally, at very slow exchange rates (high volumes and low diffusion) the membrane recruitment dips again, toward its nondiffusive value. The settling time of the output for the PKC system was faster than for PKA (Fig. 3 *F*). Responses of volumes of 10 fl and above converged to deterministic levels within 10 s.

CaMKII

The CaMKII signaling pathway is especially important for synaptic signaling. The kinase is present at very high levels in the mammalian postsynaptic region, and its activation is rather complex, involving autophosphorylation and translocation from the cytosol to the postsynaptic density upon autophosphorylation. In this study we modeled its bidirectional regulation by Ca^{2+}, involving calcineurin (CaN) as well as calcium calmodulin (CaM). We also modeled its dephosphorylation by protein phosphatase 1

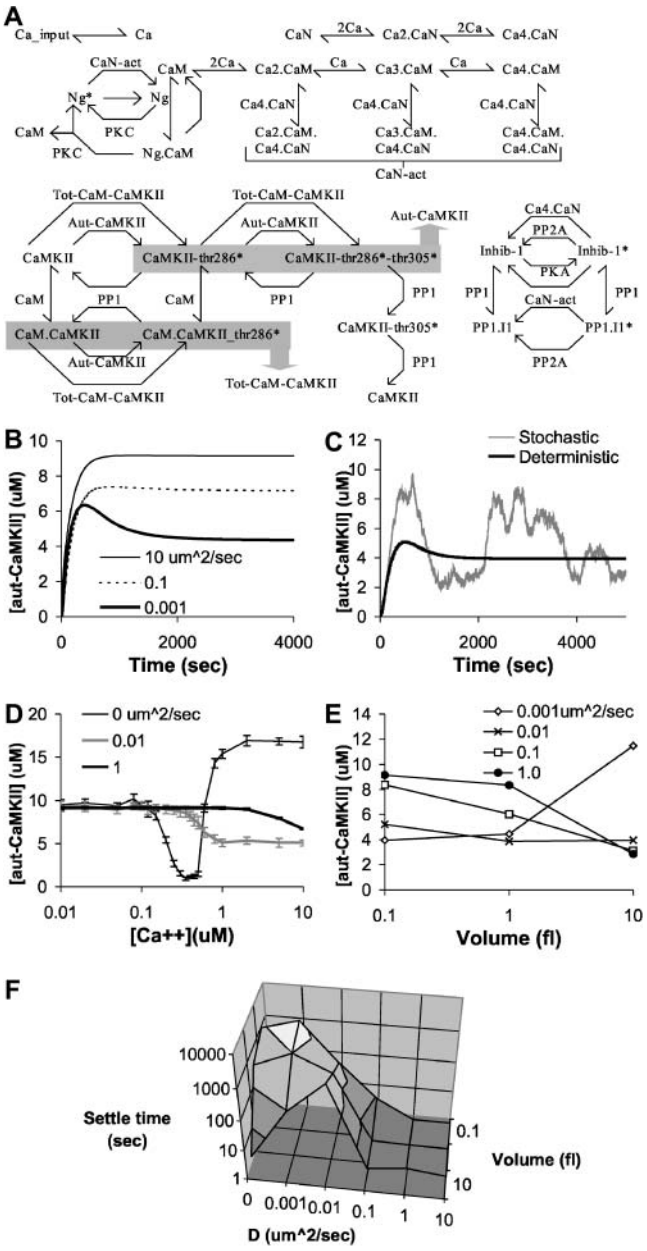

FIGURE 4 CaMKII (autonomous) responses. (*A*) Reaction scheme. Shaded blocks represent states of CaMKII whose activity is summed to give the level of autonomous CaMKII (Aut-CaMKII) and total CaM-activated CaMKII (Tot-CaM-CaMKII), respectively. CaMKII can be phosphorylated on threonine 286 (Thr-286) and threonine 305 (Thr-305) in this model. Abbreviations: CaM, calmodulin; CaN, calcineurin; CaN-act, total activated calcineurin, which is the sum of several sub-states with different levels of calcium bound to CaM; Ng, neurogranin; PP2A, protein phosphatase 2A; PP1, protein phosphatase 1; and I1, inhibitor 1. Asterisks represent phosphorylation. (*B*) Time course of simulation responses to an input of 5 μM Ca^{2+} at volume = 0.1 fl, and a range of diffusion constants. A transient response is seen at a low diffusion constant of 0.001 μm^2/s. (*C*) Comparison of stochastic and deterministic runs for identical conditions. Stimulus = 1 μM Ca^{2+}, volume = 0.1 fl, D = 0.001 μm^2/s. Note large fluctuations in stochastic run. (*D*) Dose-response curves for autonomous CaMKII with different diffusion constants in a volume of 0.1 fl. Error bars are standard deviations. Note the complex triphasic response at zero diffusion. (*E*) Washout as a function of volume and diffusion constant. Note recruitment as well as washout effects and their dependence on volume and diffusion constant. (*F*) Settling time (defined in methods) as a function of volume and diffusion constant. Note complex shape of surface, showing interaction of diffusive and chemical contributions to stochasticity.

(PP1) (Fig. 4 *A*). These pathways have additional regulatory inputs from PKA and PKC, but these kinase inputs were held constant for the purposes of this analysis and only Ca^{2+} was varied. As with the PKC model, the Ca^{2+} input was given through an intermediate rapid reaction so that the compartmental Ca^{2+} concentration could fluctuate due to stochasticity in the influx process, intrinsic Ca buffers, and diffusion. Some aspects of CaMKII regulation were included in separate simulations below. For example, the autonomous form of CaMKII (CaMKII-thr286*-thr305* in the model) also undergoes trafficking between the cytosol and the postsynaptic density (Strack and Colbran, 1998; Bayer and Schulman, 2001), and there are reports of selective enrichment of PP1 in the PSD (Strack et al., 1997). In our calculations, all molecules in the current pathway were regarded as freely diffusing between the subcellular compartment and the bulk cell body. We considered two readouts of CaMKII activity: the directly Ca-stimulated forms (Tot-CaM-CaMKII) and the Ca-autonomous forms (Aut-CaMKII). Due to the rapid kinetics and high concentrations of CaM and CaMKII, it was numerically very expensive to simulate large volumes, and we restricted our analysis to the range 0.1–10 fl.

The time course of activation of aut-CaMKII at different diffusion rates is illustrated in Fig. 4 *B*. The 0.001 μm^2/s case exhibits a transient peak in its response. This is due to the initial formation of signaling products and their subsequent washout. This was verified using separate test simulations where Aut-CaMKII was diffusionally restricted to the PSD, in which case it underwent a buildup (below). A similar washout is seen at large volumes in further simulations shown in the supplementary material. The range of steady values for the remaining curves are interesting, as they reflect a combination of washout of signaling intermediates and resupply of the inactive molecules from the bulk solution. The washout effects are analyzed below.

At synaptic volumes (0.1 fl) the autonomous CaMKII activity undergoes large, low-frequency fluctuations with much smaller high-frequency variability superimposed (Fig. 4 *C*). The large fluctuations are due to the very low steady-state levels of Ca4.CaM, which are at ~73 nM or ~0.44 molecules in 0.1 fl with the applied stimulus of 1 μM Ca^{2+}. Stochastic increases in the Ca4.CaM levels are strongly amplified by the autophosphorylation to give rise to the large fluctuations. At larger volumes the stochastic response is almost identical to the deterministic one, and the scatter is also very small (supplementary material). This is expected as the high concentrations of CaMKII lead to large numbers of interacting molecules, and converge to the deterministic limit even at moderate volumes.

The next analysis was the dose-response curves at a range of diffusion constants (Fig. 4 *D*). Here the responses of autonomous CaMKII were qualitatively different at different values of the diffusion constant from 0 to 1 $\mu m^2/s$, for a fixed volume of 1 fl. At the zero diffusion limit, the response is triphasic, in keeping with the expected profile of calcium dependence. Below 0.5 μM Ca^{2+} there is little response. There is a dip in activity around 0.5 μM Ca^{2+}. This is due to increased activity of CaN, which then increases activity of PP1 by dephosphorylating the high-affinity form of the PP1 inhibitor I1 (Fig. 4 *A*). This effect is overtaken, at ~1 μM Ca^{2+}, by the direct stimulation of CaMKII by Ca binding to CaM. This triphasic response of intermediate activity at low Ca^{2+}, decreased activity at moderate Ca^{2+}, and high activity at high Ca^{2+}, is similar to proposed calcium-dependence of bidirectional synaptic modification. It is intriguing that this response only occurs at the high-volume/low-diffusion limit, and is not observed under the small-volume conditions of the synapse. This issue is considered in the discussion section. At intermediate diffusion levels of 0.01 $\mu m^2/s$ the Aut-CaMKII response actually declines at higher Ca^{2+}. At high diffusion rates the kinase exhibits very little calcium dependence. At this volume of 1 fl the stochastic nose is small. A complex interdependence of diffusive effects with the calcium response is also observed if the volume is varied while keeping diffusion constant fixed, and for small volumes the Aut-CaMKII responses are somewhat obscured by biochemical noise (supplementary data).

The dependence of standard deviation on volume and diffusion is small, and the standard deviation values are negligible in most cases as expected from the high concentrations of CaMKII (supplementary data). However, these curves do not take into account the low stimulus case of Fig. 4, *D* and *F*, where there is a very large variability.

The diffusive interchange of elements of the CaMKII pathway leads to interesting effects as seen in Fig. 4 *E*. At all but the smallest diffusion rates, there is a decline in autonomous CaMKII activity with increasing volume. In the case where there is a large 10 fl compartment nearly but not completely isolated from the bulk cytosol, the system reverts to the nondiffusive limit and exhibits a larger response at this Ca level. This is equivalent to the high portion of the triphasic response in Fig. 4 *D*.

The settling profile of autonomous CaMKII is also unusual. There is a very large dependence on diffusion constant. At high diffusion rates the responses settle almost immediately. At zero diffusion rates there is the expected dependence of settling times on volume, where the averaged CaMKII activity at larger volumes converges very quickly to the deterministic activity. However, at intermediate diffusion rates there is a rise in settling time. This is due to the near-washout of low concentration regulatory molecules, especially Ca4.CaM from the compartment, leading to a very large variation in autonomous CaMKII levels. This effect is also seen in Fig. 4 *C*.

Whereas autonomous CaMKII exhibits numerous deviations from deterministic, single-compartment response profiles, the directly CaM-activated state of CaMKII behaves in a very predictable manner. There are severe washout effects at small volumes and high diffusion rates (Fig. 5, *A* and *D*). The stochastic fluctuations about the deterministic response are relatively high-frequency and in a narrow band (Fig. 5 *B*; supplementary material). The dose-response curves again exhibit the expected washout profile, and high diffusion rates (Fig. 5 *C*) and small volumes (supplementary material) and both have their Ca^{2+} dependence shifted over to the right. Finally, the convergence of the average of the response to the deterministic response occurs quickly even at only 1 fl, and has relatively little diffusion dependence. This simple behavior is probably due to the relatively high K_d of calcium dependence of CaM (~1 μM) and simple stoichiometric reaction sequence of CaMKII, unlike the

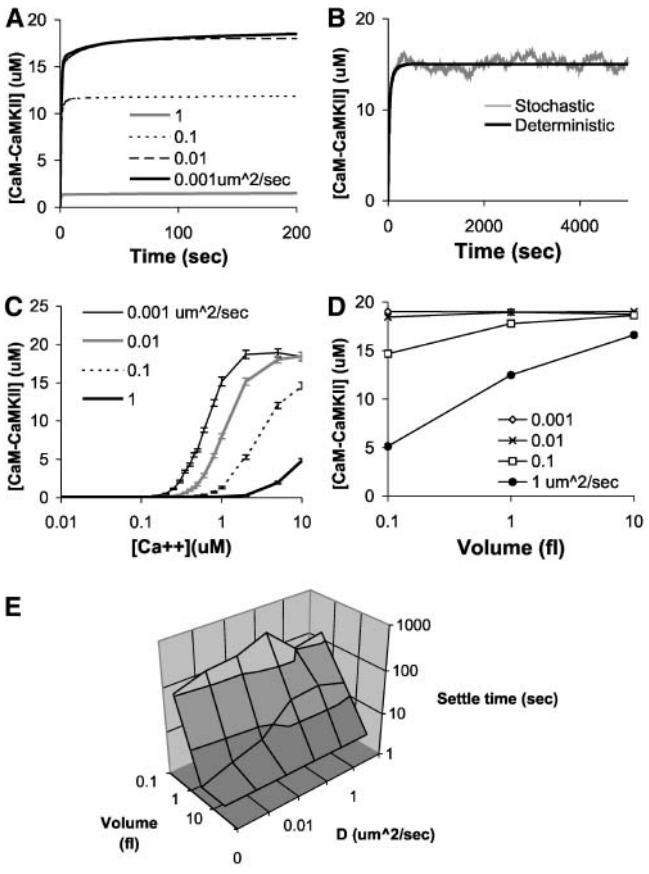

FIGURE 5 CaMKII (CaM-activated) responses. (*A*) Time course of simulation responses to an input of 5 μM Ca^{2+} at volume = 0.1 fl, and a range of diffusion constants. (*B*) Comparison of stochastic and deterministic runs for stimulus = 1 μM Ca^{2+}, volume = 0.1 fl, D = 0.001 $\mu m^2/s$. (*C*) Dose-response curves for autonomous CaMKII with different diffusion constants in a volume of 0.1 fl. Error bars are standard deviations. (*E*) Washout as a function of volume and diffusion constant. (*F*) Settling time (defined in methods) as a function of volume and diffusion constant.

much more complicated activation of autonomous CaMKII (Fig. 4 *A*).

MAPK

The MAPK cascade is the prototypical high-gain, slow-acting signaling pathway and has many important cellular effects. The activated form of MAPK (MAPK* in Fig. 6 *A*) is doubly phosphorylated, and its upstream activator kinase (MEK) is also doubly phosphorylated, thus giving rise to high apparent order of reaction for the cascade. MAPK is abundant at the synapse (Ortiz et al., 1995) and thus its low-volume behavior is likely to be of interest. In this model we regard the EGFR complexes, the Ras complexes and the GTP.Ras.cRaf* complex as being membrane-anchored (Fig. 6 *A*). The remaining molecules are freely diffusing. There are numerous reports of scaffolding proteins anchoring portions of the MAPK cascade, and some of the signaling consequences of scaffolding have been analyzed previously (Levchenko et al., 2000; Morrison and Davis, 2003). The epidermal growth factor (EGF) signaling pathway also undergoes endocytosis, which presents its own interesting dynamics (Resat et al, 2003). An analysis of scaffolding effects and endocytosis is outside the scope of this study. Here we apply EGF at a range of concentrations and monitor MAPK activity.

The MAPK deterministic and low diffusion response is a transient (Fig. 6 *B*), due both to receptor internalization and negative feedback from the active MAPK to upstream steps in the pathway (Fig. 6 *A*). There is a very strong washout evident at small volumes and high diffusion rates, and the response falls to nearly zero under these conditions (Fig. 6 *B*). Basal MAPK activity is low, and the activity of individual molecules is comparable to the basal deterministic activity (Fig. 6 *C*). Consequently fluctuations in the MAPK response are large compared to the deterministic response. As was the case with PKA, the high amplification of the cascade can lead to single-channel like large transient activity much greater than the deterministic activity of the kinase (Fig. 6 *C*).

The stochastic dose-response curves for MAPK could not be obtained from individual simulation runs because of the transient nature of the response. Therefore the distribution of MAPK responses was obtained by taking the peak response from 30 individual runs under each combination of stimulus, volume and diffusion constant. The dose-response curves reflect the high gain and small molecule count of stages in the cascade. At very low volumes the MAPK response is large and very noisy, and quite independent of EGF levels (supplementary material). EGF-dependent responses manifest only at volumes over 100 fl, and are still highly suppressed by washout. The strong washout is also seen in Fig. 6 *D*, where the response is almost completely suppressed except at diffusion rates of 0.01 $\mu m^2/s$ or lower. It is only at high volumes and low diffusion rates that a strong EGF-stimulated response can be elicited from MAPK under the assumptions of this model.

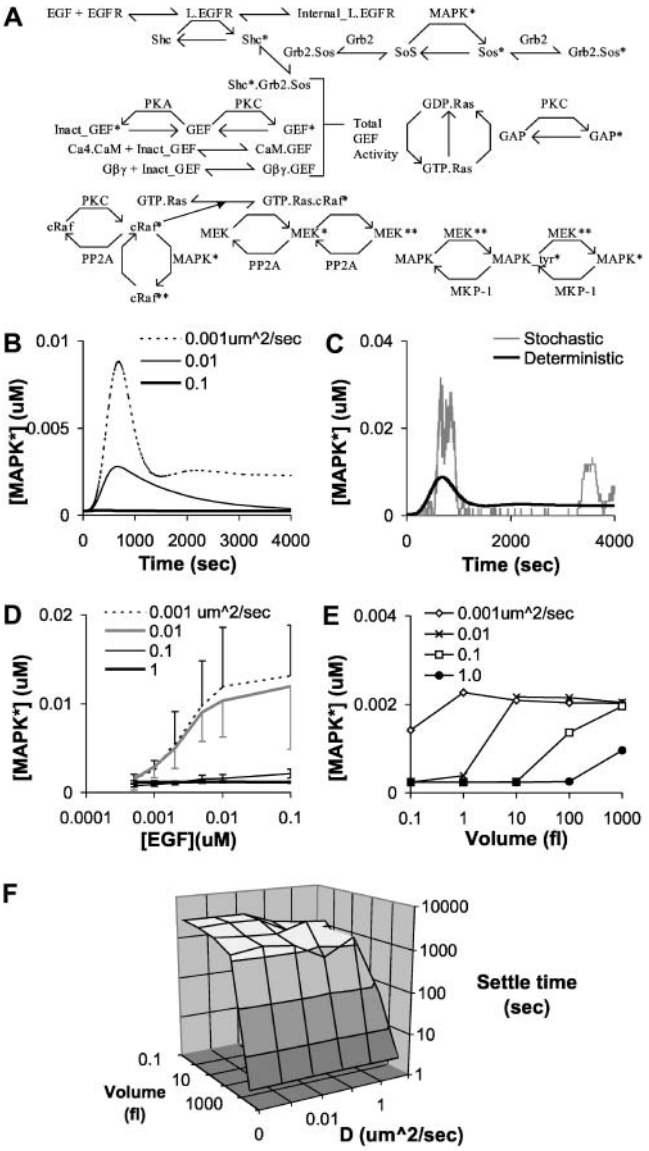

FIGURE 6 MAPK responses. (*A*) Reaction scheme. Abbreviations: EGF, epidermal growth factor; EGFR, EGF receptor; L.EGFR, EGF bound form of EGFR; GEF, guanine nucleotide exchange factor; GAP, GTPase activating protein; MEK, MAPK kinase; MKP-1, MAP kinase phosphatase type 1; MAPK_tyr*, tyrosine phosphorylated MAPK; and MAPK*, doubly phosphorylated and active MAPK. Phosphorylation states are indicated by asterisks. (*B*) Time course of simulation responses to an input of 100 nM EGF at volume = 1 fl, and a range of diffusion constants. Washout occurs for a diffusion constant of 0.1 $\mu m^2/s$. (*C*) Comparison of stochastic and deterministic runs for stimulus = 100 nM EGF, volume = 1 fl, $D = 0.001$ $\mu m^2/s$. Note large fluctuations in stochastic run. (*D*) Dose-response curves for MAPK with different diffusion constants in a volume of 10 fl. Error bars are standard deviations. (*E*) Washout as a function of volume and diffusion constant. (*F*) Settling time (defined in methods) as a function of volume and diffusion constant. Note long setting time for all volumes except 1000 fl.

The standard deviation of the response declines as expected with increasing volume, but there is a small

increase at large volumes (supplementary material). This is due to the reduction in washout at large volumes, and the consequent increase in concentrations of activated MAPK. The profound effect of washout on the MAPK response is summarized in Fig. 6 *E*. The responses of the pathway are essentially at baseline whenever there is rapid diffusional coupling with the bulk cytosol. This is not surprising, as the MAPK pathway has a rather slow response time (Fig. 6 *B*), making it more susceptible to washout.

The time required for the averaged MAPK response to settle to the deterministic value was computed using a slight variation on the calculation described in the methods. Instead of averaging over a range of stimulus amplitudes, the settling time was averaged over 15 independent simulation runs because the variability was large. Additionally, a threshold of 0.1 rather than 0.05 was used. As expected, MAPK responses have to be integrated for rather long periods to obtain accurate readouts (Fig. 6 *F*). It is only at volumes comparable to an entire cell that the settling time is rapid. This limitation may not be as severe as for the other pathways, because the MAPK response is already a slow one and downstream pathways may therefore have evolved to integrate over long periods. There is relatively little diffusion dependence of the MAPK settling time.

Compartmentalization and membrane anchoring

The profound influence of washout on the above simulations suggested that relatively small changes in the membrane anchoring status of molecules might lead to interesting changes in the pathway behavior. This was investigated for hypothetical situations in the PKA and CaMKII pathways respectively. For the PKA pathway, the behavior of the GTP.Gα molecule was changed from membrane-anchored to freely diffusing. This change converted a slowly settling response (Figs. 7 *A* and 2 *E*) to a transient response (Fig. 7 *B*). The initial rapid buildup of GTP.Gα due to ligand stimulation washes out and the eventual PKA response is low.

In the case of the CaMKII pathway, the proposed subcellular localization of autonomous CaMKII and PP1 to the PSD was considered (Strack et al., 1997; Bayer and Schulman, 2001). This change led to a runaway feedback of autonomous CaMKII for Ca^{2+} inputs above a threshold of $\sim$0.35 μM (Fig. 7 *D*). In the original model there is very little difference between the autonomous CaMKII activity for Ca^{2+} at 0.3 or 0.4 μM. With the localization to the PSD, the 0.4 μM Ca^{2+} case diverges strongly from the 0.3 μM case. The effect is due to the substrate saturation of PP1, which is now restricted to the PSD along with large amounts of autophosphorylated CaMKII. As PP1 cannot diffuse in from the bulk, there is a limit to the maximal rate at which PP1 can dephosphorylate CaMKII and hence remove it from the PSD. CaMKII, on the other hand, can diffuse freely into the compartment from the bulk in its dephosphorylated state.

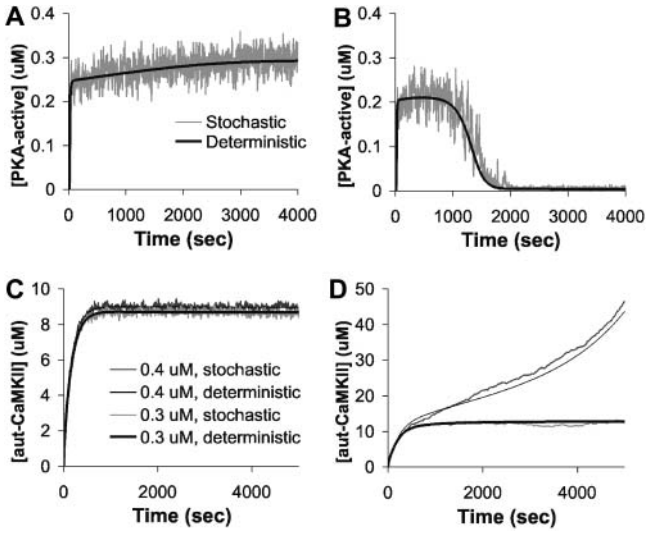

FIGURE 7 Membrane anchoring effects. (*A*) Stochastic and deterministic responses of PKA to a steady stimulus of 0.1 μM ligand in a volume of 1fl at $D = 0.1$ $\mu m^2/s$, as in Fig. 2 *E*. (*B*) Same conditions except that the GTP.Gα molecule is now diffusive. There is now a transient response. (*C*) Stochastic and deterministic responses of autonomous CaMKII in a volume of 1 fl at $D = 0.1$ $\mu m^2/s$, using two stimuli each of 0.3 and 0.4 μM Ca^{2+}. (*D*) Same conditions except that the autonomous CaMKII and PP1 are now treated as anchored to the PSD. There is a runaway buildup of autonomous CaMKII in the 0.4 μM case.

When the Ca^{2+} stimulus is large enough, the balance between the limited PP1 dephosphorylation and the nearly unlimited supply of autophosphorylated CaMKII tips, and there is runaway buildup. This effect is similar to zero-order hypersensitivity (Goldbeter and Koshland, 1981).

DISCUSSION

This study examines responses of four selected signaling pathways in small subcellular compartments in diffusive contact with the rest of the cell. Stochasticity and diffusion combine to give response properties markedly at variance with the outcomes of deterministic signaling in well-stirred single compartments. The major outcome of stochasticity is to introduce molecular ''noise'' that obscures signaling especially at small volumes. Diffusion frequently interacts strongly with this ''noise'' term, and could either increase or decrease the effective molecular noise depending on context. Diffusion also obscured signaling outcomes at small volumes, often leading to washout of responses, but in some cases reinforcing or qualitatively changing the response profiles.

Volume scaling and reliability of signaling

These simulations were performed over a range of simulated ''volumes'' from 1000 to 0.1 fl, in diffusive contact with a cell of 1000 fl. The compartment volume range is from medium-sized cells (10 μm diameter) to large organelles and

cellular subcompartments such as synapses (0.1 μm diameter). For reference, an *Escherichia coli* is ~3 fl in volume. Our simulations simply scale all molecule numbers linearly with volume, based on a set of initial concentrations obtained from the experimental literature (supplementary material). This is obviously a crude approximation, given that organelles and cellular compartments almost by definition have a distinct molecular composition and that membrane area scales as volume$^{(2/3)}$. Further, our diffusion constants are the same for all molecules except those that are membrane-anchored. Nevertheless, it may be valuable to have a semiquantitative understanding of scaling effects on signaling, and these simulation results lend themselves to such an interpretation. Fig. 8 summarizes the qualitative conclusions about reliability of signaling of different pathways as a function of volume. It is clear that for most signaling pathways, diffusively-coupled mass-action signaling ceases to be computationally reliable at ~1 fl and below. For example, the classical logic of signaling may be inapplicable to most of the events in the postsynaptic dendritic spine. This is entirely consistent with the emerging body of evidence concerning protein scaffolds, cytoskeletal complexes, and signal channeling, which come into play precisely at these smaller volumes (reviewed in Smith and Scott, 2002).

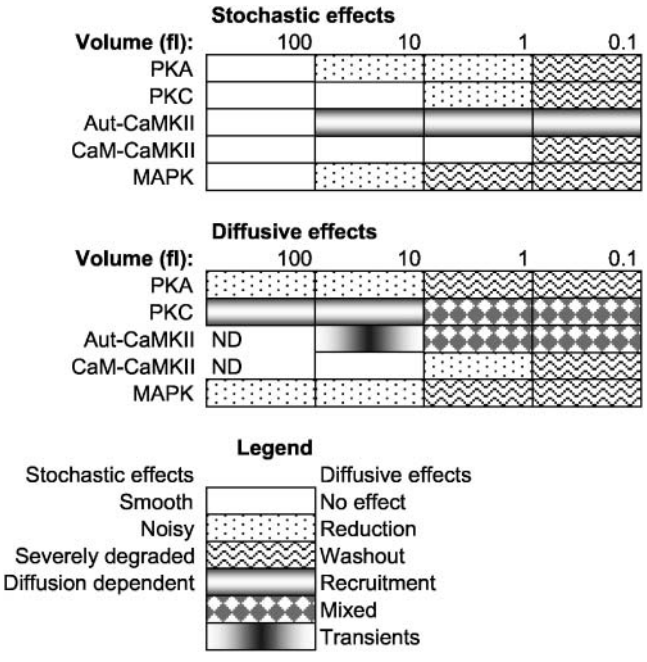

FIGURE 8 Summary of stochastic and diffusive effects as a function of volume. ''Severely degraded'' indicates that the scatter or distortion in signaling response is so severe as to render the pathway output uninformative for downstream signaling. In the case of diffusive responses, ''mixed'' indicates that the response includes both washout and recruitment effects.

Diffusive modulation of signaling

A second implication of this study is that a combination of membrane/cytoskeletal targeting and diffusive coupling between compartments can lead to computationally interesting effects on signaling outcomes. Some related effects have previously been proposed for kinase-phosphatase systems (Kholodenko, 2003). Protein targeting is well known to be important in signaling effects, especially at the synapse (Meyer and Shen, 2000; Shen et al., 2000). This study considers diffusive effects in the context of rather detailed models of signaling cascades with the goal of understanding such effects in a biologically constrained setting. We encountered at least four distinct outcomes depending on a combination of localization of molecules in space and in the signaling cascade. In each case the small volume of the signaling system is important because it brings the diffusion rates into the same range as the chemical rates.

The first, and simplest, outcome is washout of signal. This occurs for all of the cascades in this study to some degree (Figs. 2 *E*, 5 *E*, and 6 *E*). In most cases the model assumes that the activated molecule is diffusible, and the washout occurs whenever the rate of diffusion exceeds rate of formation of the molecule.

The second outcome is superficially the converse of washout: recruitment to the membrane. This occurs for PKC where the active form is assumed to be membrane anchored. The effect is more interesting than simple recruitment in this example, because it competes with a washout effect of earlier stages in the PKC activation pathway. The net result is a multiphasic response (Fig. 3 *E*).

The third outcome is a transient activation of a pathway (Fig. 7 *B*). This occurs for a version of the PKA model where we allow GTP.Gα to diffuse. Whereas this specific reaction is unphysiological, similar contexts may occur when an intermediate in an activation cascade is diffusible. Transient responses are important in biology, and are typically interpreted as due to an active negative feedback process such as receptor inactivation or internalization. It is interesting that here it occurs purely due to a biophysical process of diffusion rather than through additional chemical steps. As before, the transient response depends on a balance between diffusive rates and chemical rates that takes effect at small signaling volumes.

The fourth outcome is a runaway accumulation of autophosphorylated CaMKII at the postsynaptic density (Fig. 7 *D*). The basis for this situation is stimulus-dependent accumulation, coupled with rate-limited removal of a molecule. For this to occur, it is necessary that the diffusive influx of the molecule can occur faster than the rate-limiting step of removal. It is interesting that this behavior is quite close to some experimentally-based proposals for this signaling pathway (Meyer and Shen, 2000). However, additional chemical regulatory steps are clearly required to keep the response in the physiological range.

This variety of diffusion- and volume-dependent effects may lead to interesting issues in growing and motile cells. For example, over a physiological range of subcellular volumes and diffusive coupling, the same pathway may switch from washout to recruitment to isolation. This highlights the importance of cellular context in understanding signaling outcome. Overall, the interplay between stochasticity and diffusion at small volumes sets many constraints on possible signaling mechanisms due to effects of noise and signal washout. On the other hand, it also opens up several additional possible mechanisms for interesting signaling computations due to the convergence of diffusive and chemical timescales.

SUPPLEMENTARY MATERIAL

An online supplement to this article can be found by visiting BJ Online at http://www.biophysj.org.

The author acknowledges the programming work by Karan Vasudeva in implementing numerical methods used in this project, and useful comments by J. Mishra and S. M. Ajay.

This work was supported by funds from National Centre for Biological Sciences, Tata Institute of Fundamental Research, and an International Senior Research Fellowship from the Wellcome Trust to U.S.B.

REFERENCES

Arkin, A., J. Ross, and H. H. McAdams. 1998. Stochastic kinetic analysis of developmental pathway bifurcation in phage lambda-infected Escherichia coli cells. *Genetics*. 149:1633–1648.

Bayer, K. U., and H. Schulman. 2001. Regulation of signal transduction by protein targeting: the case for CaMKII. *Biochem. Biophys. Res. Commun.* 289:917–923.

Berg, O. G., J. Paulsson, and M. Ehrenberg. 2000. Fluctuations and quality of control in biological cells: zero-order ultrasensitivity reinvestigated. *Biophys. J.* 79:1228–1236.

Bhalla, U. S. 1998. The network within: signaling pathways. *In* The Book of GENESIS: Exploring Realistic Neural Models with the GEneral NEural SImulation System. J. M. Bower and D. Beeman, editors. Springer-Verlag, New York. 169–190.

Bhalla, U. S. 2002a. Mechanisms for temporal tuning and filtering by postsynaptic signaling pathways. *Biophys. J.* 83:740–752.

Bhalla, U. S. 2002b. Use of Kinetikit and GENESIS for modeling signaling pathways. *In* Methods in Enzymology. J. D. Hildebrandt and R. Iyengar, editors: Academic Press, New York. 3–23.

Bower, J. M., and D. Beeman. 1998. The Book of GENESIS. Springer-Verlag, New York.

Elowitz, M. B., A. J. Levine, E. D. Siggia, and P. S. Swain. 2002. Stochastic gene expression in a single cell. *Science*. 297:1183–1186.

Falcke, M. 2003. On the role of stochastic channel behavior in intracellular Ca2+ dynamics. *Biophys. J.* 84:42–56.

Fink, C.C., B. Slepchenko, I. I. Moraru, J. Watras, J. C. Schaff, and L. M. Loew. 2000. An image-based model of calcium waves in differentiated neuroblastoma cells. *Biophys. J.* 79:163–183.

Franks, K. M., T. M. J. Bartol, and T. J. Sejnowski. 2002. A Monte Carlo model reveals independent signaling at central glutamatergic synapses. *Biophys. J.* 83:2333–2348.

Gibson, M. A., and J. Bruck. 2000. Efficient exact stochastic simulation of chemical systems with many species and many channels. *J. Phys. Chem. A.* 104:1876–1889.

Gillespie, D. T. 1977. Exact stochastic simulation of coupled chemical reactions. *J. Phys. Chem.* 81:2340–2361.

Goldberg, J. H., G. Tamas, D. Aronov, and R. Yuste. 2003. Calcium microdomains in aspiny dendrites. *Neuron*. 40:807–821.

Goldbeter, A., and D. E. Koshland, Jr. 1981. An amplified sensitivity arising from covalent modification in biological systems. *Proc. Natl. Acad. Sci. USA*. 78:6840–6844.

Gonze, D., J. Halloy, and A. Goldbeter. 2002. Robustness of circadian rhythms with respect to molecular noise. *Proc. Natl. Acad. Sci. USA*. 99:673–678.

Harrison, L. G. 1993. Kinetic Theory of Living Pattern. Cambridge University Press, Cambridge.

Kepler, T. B., and T. C. Elston. 2001. Stochasticity in transcriptional regulation: origins, consequences, and mathematical representations. *Biophys. J.* 81:3116–3136.

Kholodenko, B. N. 2003. Four-dimensional organization of protein kinase signaling cascades: the roles of diffusion, endocytosis and molecular motors. *J. Exp. Biol.* 206:2073–2082.

Kholodenko, B. N., G. C. Brown, and J. B. Hoek. 2000. Diffusion control of protein phosphorylation in signal transduction pathways. *Biochem. J.* 350:901–907.

Kierzek, A. M., J. Zaim, and P. Zielenkiewicz. 2001. The effect of transcription and translation initiation frequencies on the stochastic fluctuations in prokaryotic gene expression. *J. Biol. Chem.* 276: 8165–8172.

Levchenko, A., J. Bruck, and P. W. Sternberg. 2000. Scaffold proteins may biphasically affect the levels of mitogen-activated protein kinase signaling and reduce its threshold properties. *Proc. Natl. Acad. Sci. USA*. 97:5818–5823.

Levin, M. D., T. S. Shimizu, and D. Bray. 2002. Binding and diffusion of CheR molecules within a cluster of membrane receptors. *Biophys. J.* 82:1809–1817.

MacGregor, R. J. 1987. Neural and Brain Modeling. Academic Press, San Diego.

Meyer, T., and K. Shen. 2000. In and out of the postsynaptic region: signaling proteins on the move. *Trends Cell Biol.* 10:238–244.

Morrison, D. K., and R. J. Davis. 2003. Regulation of MAP kinase signaling modules by scaffold proteins in mammals. *Annu. Rev. Cell Dev. Biol.* 19:91–118.

Morton-Firth, C. J., T. S. Shimizu, and D. Bray. 1999. A free-energy-based stochastic simulation of the Tar receptor complex. *J. Mol. Biol.* 286: 1059–1074.

Ortiz, J., H. W. Harris, X. Guitart, R. Z. Terwillinger, J. W. Haycock, and E. J. Nestler. 1995. Extracellular signal-regulated protein kinases (ERKs) and ERK Kinase (MEK): Regional distribution and regulation by chronic morphine. *J. Neurosci.* 15:1285–1297.

Ozbudak, E. M., M. Thattai, I. Kurster, A. D. Grossman, and A. van Oudenaarden. 2002. Regulation of noise in the expression of a single gene. *Nat. Genet*. 31:69–73.

Paulsson, J., O. G. Berg, and M. Ehrenberg. 2000. Stochastic focusing: fluctuation-enhanced sensitivity of intracellular regulation. *Proc. Natl. Acad. Sci. USA*. 97:7148–7153.

Rao, C. V., D. M. Wolf, and A. P. Arkin. 2002. Control, exploitation and tolerance of intracellular noise. *Nature*. 420:231–237.

Resat, H., J. A. Ewald, D. A. Dixon, and H. S. Wiley. 2003. An integrated model of epidermal growth factor receptor trafficking and signal transduction. *Biophys. J.* 85:730–743.

Rich, T. C., K. A. Fagan, H. Nakata, J. Schaack, D. M. Cooper, and J. W. Karpen. 2000. Cyclic nucleotide-gated channels colocalize with adenylyl cyclase in regions of restricted cAMP diffusion. *J. Gen. Physiol.* 116:147–161.

Sabatini, B. L., and K. Svoboda. 2000. Analysis of calcium channels in single spines using optical fluctuation analysis. *Nature*. 408:589–593.

Shen, K., M. N. Teruel, J. H. Connor, S. Shenolikar, and T. Meyer. 2000. Molecular memory by reversible translocation of calcium/calmodulin-dependent protein kinase II. *Nat. Neurosci.* 3:881–886.

Shimizu, T. S., S. V. Aksenov, and D. Bray. 2003. A spatially extended stochastic model of the bacterial chemotaxis signaling pathway. *J. Mol. Biol.* 329:291–309.

Sivakumaran, S., S. Hariharaputran, J. Mishra, and U.S. Bhalla. 2003. The database of quantitative cellular signaling: management and analysis of chemical kinetic models of signaling networks. *Bioinformatics.* 19:408–415.

Smith, F. D., and J. D. Scott. 2002. Signaling complexes: junctions on the intracellular information super highway. *Curr. Biol.* 12:32–40.

Stiles, J. R., and T. M. Bartol. 2000. Monte Carlo methods for simulating realistic synaptic microphysiology using mcell. *In* Computational Neuroscience: Realistic Modeling for experimentalists. E. De Schutter, editor. CRC Press, Boca Raton, FL. 87–128.

Strack, S., M. A. Barban, B. E. Wadzinski, and R. J. Colbran. 1997. Differential inactivation of postsynaptic density-associated and soluble Ca2+/Calmodulin-dependent protein kinase II by protein phosphatases 1 and 2A. *J. Neurochem.* 68:2119–2128.

Strack, S., and R. J. Colbran. 1998. Autophosphorylation-dependent targeting of calcium/calmodulin-dependent protein kinase II by the NR2B subunit of the N-methyl- D-aspartate receptor. *J. Biol. Chem.* 273:20689–20692.

Strier, D. E., A. C. Ventura, and S. P. Dawson. 2003. Saltatory and continuous calcium waves and the rapid buffering approximation. *Biophys. J.* 85:3575–3586.

Thattai, M., and A. van Oudenaarden. 2001. Intrinsic noise in gene regulatory networks. *Proc. Natl. Acad. Sci. USA.* 98:8614–8619.

Vasudeva, K., and U. S. Bhalla. 2004. Adaptive stochastic-deterministic chemical kinetic simulations. *Bioinformatics.* 20:78–84.

Vilar, J. M., H. Y. Kueh, N. Barkai, and S. Leibler. 2002. Mechanisms of noise-resistance in genetic oscillators. *Proc. Natl. Acad. Sci. USA.* 99: 5988–5992.